Title

Depletion of phagocytic cells during nonlethal *Plasmodium yoelii* infection causes severe malaria characterized by acute renal failure in mice

Running title

Role of phagocytic cells in malaria

Authors

Mohamad Alaa Terkawi[a †], Maki Nishimura[a †], Hidefumi Furuoka[b], Yoshifumi Nishikawa[a]

Affiliations

[a]National Research Center for Protozoan Diseases, Obihiro University of Agriculture and Veterinary Medicine, Obihiro, Japan.

[b]Department of Basic Veterinary Medicine, Obihiro University of Agriculture and Veterinary Medicine, Obihiro, Japan.

Correspondence

Yoshifumi Nishikawa (PhD)

Tel: +81-155-49-5641

Fax: +81-155-49-5643

E-mail: nisikawa@obihiro.ac.jp

[†]Both authors contributed equally to this work.

Abstract

In the current study, we examined the effects of phagocytes depletion on the progression of *Plasmodium yoelii*-17XNL infection in mice. Strikingly, the depletion of phagocytic cells, including macrophages with clodronate in the acute-phase of infection significantly reduced peripheral parasitemia but increased mortality. Moribund mice displayed severe pathological damages included coagulative necrosis in liver and thrombi in the glomeruli, fibrin deposition, and tubulonecrosis in kidney. The severity of infection was coincident with the increased sequestration of parasitized erythrocytes, the systematic upregulation of inflammation and coagulation, and the disruption of endothelial integrity in the liver and kidney. Aspirin was administered to the mice to minimize the risk of excessive activation of the coagulation response and fibrin deposition in the renal tissue. Interestingly, treatment with aspirin reduced the parasite burden and pathological lesions in the renal tissue and improved survival of phagocyte-depleted mice. Our data imply that the depletion of phagocytic cells, including macrophages in the acute-phase of infection increases the severity of malarial infection, typified by multiorgan failure and high mortality.

Key words: Phagocytes; macrophages; phagocytosis; *Plasmodium yoelii*.

Introduction

Malaria remains the most devastating protozoan infection in the world, with a heavy disease burden estimated to affect 300-500 million individuals, with 0.6 million deaths annually. *Plasmodium falciparum* is the most important etiological agent of malaria, causing high levels of morbidity and mortality worldwide. The severity of infection is broad ranging, from a slight febrile illness to severe complications, which can include cerebral malaria, acidosis, acute respiratory distress syndrome, and acute renal and hepatic failure [1-3]. Transmission occurs via the bite of an infected female *Anopheles* mosquito, which releases sporozoites into the bloodstream. The inoculated motile sporozoites invade the hepatocytes and replicate intracellularly. Following the clinically silent liver stage, the merozoite progeny move into the bloodstream and initiates the blood stage, which is associated with the clinical manifestations of malaria [1, 4].

The intensive replication of the parasite within the erythrocytes (red blood cells, RBCs) and the exportation of parasite proteins to the RBC surface alter the RBC membrane characteristics, allowing RBCs to adhere to the endothelium and causing their sequestration in the blood microvessels of various organs. Parasitized erythrocytes (pRBC) can also adhere to other RBCs, leukocytes, and platelets, forming intravascular

56 rosettes and clumps, which can impede the microcirculation and disrupt the
57 microvascular blood flow, leading to hypoxia and multiorgan failure [4]. In fact,
58 disruption of the microvascular blood flow is commonly observed in experimental and
59 human clinical studies of severe malaria. Together with this sequestration, the
60 overproduction of inflammatory cytokines and soluble mediators by the host immune
61 cells at the sites of infection promote endothelial cell injury [5-7]. The loss of the
62 endothelial barrier integrity results in microvascular leakage and organ injury and
63 dysfunction. Thrombosis is triggered by the exposure of tissue factor (TF) expressed on
64 the surfaces of endothelial cells and monocytes to thrombin, leading to fibrin deposition
65 in the blood vessels and obstruction to blood flow [6, 7].

66 Efficient control of *Plasmodium* infection by the host is dependent on the
67 function of spleen via filtering pRBCs and regulating the consequence immune response
68 to the infection [8]. In the spleen, the blood leaves the terminal arterioles into sinuses of
69 marginal zone, where marginal zone macrophages and marginal metallophilic
70 macrophages are positioned at a ring form surrounding the sinus. This strategic position
71 of macrophages allows them to sufficiently trap and phagocytize blood pathogens [9,
72 10]. However, it is still unclear that splenic macrophages are crucial for the clearance of
73 the pRBC. In the present study, clodronate liposome (CLL) that is known to deplete

splenic phagocytes, mainly macrophages in marginal zone and red pulp [10, 11] was used to investigate the contribution of macrophages on the host protection against blood stage of *P. yoelii* infection in C57BL/6 mice. Our data show that resistance to nonlethal *P. yoelii* infection is crucially dependent on the function of phagocytic cells including macrophages in mice.

Materials and methods

Mice and infection: Specific-pathogen-free 6–8-week-old female C57BL/6 mice purchased from Clea (Tokyo, Japan) were used in this study. *Plasmodium yoelii* 17-XNL was recovered from frozen pRBC stock by passage in mice after intraperitoneal (i.p.) inoculation, and the challenge infections were induced with i.p. inoculations of 1×10^7 fresh pRBCs from donor mice. Parasitemia and survival rates were monitored daily thereafter. Parasitemia was determined by microscope in methanol-fixed thin blood smears stained with 10% Giemsa solution. This study was performed in strict accordance with the recommendations in the Guide for the Care and Use of Laboratory Animals of Ministry of Education, Culture, Sports, Science and Technology, Japan. The protocol was approved by the Committee on the Ethics of Animal Experiments of the Obihiro University of Agriculture and Veterinary Medicine (Permit number 24-17, 25-66).

Depletion of phagocytes and treatment with aspirin: Phagocytes were depleted by the i.p. administration of 300 μl of CLL once on day –2 postinfection (p.i.) for the early-phase of infection, on day 6 p.i. for the acute-phase of infection, on day 14 p.i. for the lately acute-phase of infection, and on day 30 p.i. for the resolved-phase of infection. Another group of mice were injected in parallel with PBS liposomes (PL). Uninfected

98 mice received either CLL or PL. CCL and PL were purchased from
99 www.clodronateliposomes.org (Haarlem, the Netherlands). In a separate experiment,
100 mice infected with *P. yoelii* were injected i.p. with either 25 mg/kg aspirin
101 (acetylsalicylic acid; Sigma-Aldrich, St. Louis, MO, USA) or PBS from day 5 to day 8
102 p.i. [12]. On day 6 p.i., the mice received either CLL or PL (300 μl) by i.p. injection.
103 **Quantitative real-time polymerase chain reaction (qRT–PCR):** The mice were killed
104 and their organs harvested (including spleen, liver, kidney, lungs, heart, and brain) and
105 placed in TRI Reagent (Sigma). Total RNA was then isolated and reverse transcribed to
106 first-strand cDNA (Invitrogen, Carlsbad, CA, USA), according to manufacturer's
107 instructions. The expression of *P. yoelii* 18S rRNA (Py18S), cytokines, and adhesion
108 molecules was analyzed with qRT–PCR using an ABI Prism Genetic Analyzer (Applied
109 Biosystems, Carlsbad, CA, USA) with SYBR Green (Applied Biosystems) and the
110 specific primers (Table S1). The primers for qRT–PCR were designed with the Primer
111 Express software (Applied Biosystems). Specific gene expression was normalized to the
112 expression of ubiquitin, using β-actin, glyceraldehyde 3-phosphate dehydrogenase
113 (GAPDH), and 18S rRNA as the housekeeping genes. The optimal reference gene was
114 selected based on the Cotton EST database (http://www.leonxie.com). Relative gene
115 expression was calculated with the $\Delta\Delta^{CT}$ method (User Bulletin no. 2, Perkin-Elmer,

116 Boston, MA, USA).

117 **Detection of serum cytokines and coagulation factors:** Each mouse serum sample
118 was assayed with an enzyme-linked immunosorbent assay (ELISA) for IFN-γ, TNF-α,
119 IL-1β, IL-10 (Pierce Biotechnology, Rockford, IL, USA), prothrombin (Ptn; USCN Life
120 Science, Wuhan, China), fibrinogen (Fbg), and D-dimer (DD; BMASSY, Beijing,
121 China), according to each manufacturer's instruction.

122 **Hematology and serum biochemistry:** Blood cell counts were performed with an
123 automatic cell counter (Celltac α, Nihon Kohden, Tokyo, Japan). Serum samples for
124 biochemical analysis were examined with a clinical chemistry automated analyzer
125 (Toshiba Medical Systems Co., Tochigi, Japan) to measure the concentrations total
126 protein (TP), aspartate transaminase (AST), alkaline phosphatase (ALP), γ-glutamyl
127 transpeptidase (γ-GTP), creatinine (CRE), and blood urea nitrogen (BUN) with specific
128 detection reagents (Denka Seiken, Tokyo, Japan).

129 **Histopathology, immunohistopathology, immunofluorescence, and electron**
130 **microscopy:** Organs were fixed in 4% (w/v) buffered paraformaldehyde, embedded in
131 paraffin, sectioned to 4 μm, and then stained with hematoxylin and eosin (HE) and
132 phosphotungstic acid hematoxylin (PTAH). The immunohistochemical staining assays
133 were performed with specific antibodies directed against intercellular adhesion

134 molecule 1 (ICAM1; Sino Biological Inc., Beijing, China; diluted 1:500), von
135 Willebrand factor (vWF; Dako, Copenhagen, Denmark; diluted 1:1000), CD41 (Abcam,
136 Cambridge, MA, USA; diluted 1:500) and *P. yoelii* merozoite surface protein-1
137 (PyMSP-1/19 rabbit antiserum; Malaria Research and Reference Reagent Resource
138 Center; diluted 1:3000) as the primary antibodies. The sections were exposed to each
139 primary antibody at 4 °C overnight, and then incubated with the secondary antibody
140 conjugated to horseradish-peroxidase-labeled polymer (EnVision+ kit, Dako) for 40 min
141 at 37 °C. The signals were detected with diaminobenzidine (ImmPACT DAB®, Vector
142 Laboratories Inc., Burlingame, CA, USA), followed by counterstaining with Mayer's
143 hematoxylin. For immunofluorescence assay targeting CD41, vWF and *P. yoelii*, fresh
144 frozen tissues were sectioned to 5 μm and fixed with cold acetone. Sections were
145 exposed to each primary antibody at 4 °C overnight and then incubated with
146 Alexa-568-labeled/488-labeled goat anti-rabbit IgG antibody for 40 min at 37 °C. For
147 the ultrastructural studies with electron microscopy, kidneys fixed in 4% buffered
148 paraformaldehyde were immersed in 2.66% glutaraldehyde, postfixed in 1% osmium
149 tetroxide, embedded in resin, and processed routinely for semithin and ultrathin
150 sectioning. The sections were observed with a transmission electron microscope
151 (HT7700, Hitachi, Tokyo, Japan).

152 **Statistical analysis:** Statistical analysis was performed using GraphPad Prism 5
153 software (GraphPad Software Inc., La Jolla, CA, USA). The statistical significance of
154 differences in the parasitemia between each group of mice was analyzed by two-way
155 analysis of variance (ANOVA). Results are presented as the mean ± SEM. The
156 significance of the differences was evaluated by a one-way ANOVA followed by
157 Tukey's multiple comparisons procedure. Student's *t* test was used to compare the
158 differences between two independent groups. The significance of the differences in
159 survival was analyzed with a Kaplan–Meier nonparametric model and the curves were
160 compared using the log-rank test. Results were considered statistically significant when
161 $P < 0.05$.
162

163 **Results**

164 **Depletion of phagocytes in acute-phase of *P. yoelii* 17XNL infection causes severe**
165 **pathogenesis in C57BL/6 mice.** To examine the contribution of phagocytic cells,
166 including macrophages to the resistance to *P. yoelii* 17XNL infection, mice were treated
167 with CLL at different times during the course of infection and were monitored for their
168 parasitemia and survival. The infection of mice with *P. yoelii* 17XNL led to patent
169 parasitemia by day 2 p.i., which increased slowly, peaked by days 11–14 p.i., and
170 resolved within the fourth week of infection in mice treated with PL or not treated (Fig.
171 1A). Mice that received a single injection of CLL 2 days before infection (-2 p.i.)
172 displayed a reduction in parasitemia compared with mice treated with PL, but no
173 mortality (Fig. 1A, B). In contrast, mice that received a single injection of CLL on
174 either day 6 or day 14 p.i. showed sharp reductions in parasitemia with coincident
175 70–73% mortality (Fig. 1C–F). Mice that received a single injection of CLL or PL on
176 day 30 p.i. did not show any increase of their parasitemia with no mortality (data not
177 shown). To further gain an insight into the cellular changes in the spleen of infected
178 mice at the acute stage after treating with CLL, splenocytes of these mice were assayed
179 by flow cytometry for cell population of macrophages, dendritic cells (DC), natural
180 killer cells (NK), natural killer T cells (NKT) and T cells ($CD4^+$ and $CD8^+$). The

181 percentages of $CD11b^{+}F4/80^{+}$, $CD11c^{+}$, $CD3^{+}CD8^{+}$ cells were reduced in both
182 non-infected and infected mice after treatment with CLL (Fig. S1A and B). In addition,
183 *P. yoelii*-infected mice showed significant reduction in percentages of $Gr.1^{+}$ and
184 $CD3^{-}NK.1^{+}$, and elevation in the percentage of $CD3^{+}CD4^{+}$ cells after treatment with
185 CLL compared with those in PL-injected mice (Fig. S1B). Together, the depletion of
186 phagocytes by using CLL resulted in an alternation of cellular population of spleen in *P.*
187 *yoelii*-infected mice. These results demonstrated the absolute need for phagocytes
188 including macrophages to control acute infection of *P. yoelii* in mice. To identify the
189 mechanism underlying the pathogenesis after phagocyte depletion in the acute-phase of
190 infection (day 6 p.i.), hematological and biochemical analyses of their blood were
191 performed. Ongoing infection caused a gradual decline in the numbers of peripheral
192 RBCs and platelets and in hematocrit (HCT) values in PL-injected mice (Table. S2).
193 Strikingly, phagocyte-depleted mice displayed significantly greater numbers of RBCs
194 and platelets and higher HCT values on day 8 p.i. compared with those of mice injected
195 with PL (Table S2). These results demonstrated that the depletion of phagocyte
196 minimized the progression of anemia and thrombocytopenia caused by *P. yoelii*
197 infection. Moreover, blood levels of ALP, γ-GTP, AST, BUN, and CRE were
198 significantly elevated in the infected mice on day 7 p.i. after treatment with CLL (Fig.

199 2A). Consistently, urine test revealed increased levels of TP and CRE, but not BUN, in
200 the phagocyte-depleted mice compared with the PL-treated mice on day 7 p.i. (Fig. S2).
201 Thus, the depletion of phagocytes resulted in severe pathogenesis of a nonlethal *P.*
202 *yoelii* infection, typified by significant elevation of biochemical markers for liver and
203 kidney dysfunction in the blood and urine.

204 **Lethal infection is associated with severe pathological lesions in the liver and**
205 **kidney.** To gain better insight into the pathogenesis of the infection after the depletion
206 of phagocytes including macrophages in mice, histopathological examinations of their
207 vital organs were made. The organs were sampled from mice one day after the
208 administration of CLL on day 7 p.i., when the mice started to die. Although no marked
209 specific pathological changes were observed in the brains, hearts, lungs, or spleens of
210 the infected mice, phagocyte-depleted mice showed severe lesions in their livers and
211 kidneys (Fig. 2B–E). It is noteworthy that the histopathological lesions observed in the
212 CLL-injected mice on day 7 p.i. included focal hepatic necrosis (Fig. 2B), tubular
213 necrosis, blood stasis, thrombi, and mild fibrin deposition in the glomeruli and arterioles
214 of the kidney (Fig. 2C–E). Concurrent hepatic and renal lesions were observed in 53.3%
215 (8/15) of the infected phagocyte-depleted mice. Because histopathological observations
216 of hepatic and renal tissues were not seen in uninfected mice treated with CLL (Fig. S3),

217 the observed phenotypes were due to the parasite infection but not to the effect of CLL
218 treatment. To assess the correlation between the pathological lesions and the parasite
219 burden in the organs, we examined the parasite burdens and their localization in various
220 tissues with qRT–PCR and immunofluorescence test, respectively. Consistent with our
221 histopathological observations, the expression of Py18S gene was significantly higher in
222 the livers and kidneys of the phagocyte-depleted mice than in those of the PL-treated
223 mice (Fig. 3A, B). An immunofluorescence study using antiserum to PyMSP-1
224 demonstrated that pRBCs had accumulated in the blood vessels of the liver and the
225 glomerular capillaries of the kidney (Fig. 3C, D). To obtain direct evidence that the
226 accumulation of pRBCs in the blood vessels of the glomeruli in moribund mice led to
227 pathological lesions, the renal tissues were examined with transmission electron
228 microscopy. Notably, the glomerular capillaries appeared to be dilated and filled with
229 RBCs, pRBCs, and degenerate pRBCs (dpRBCs) (Fig. 3E). The pRBCs and dpRBCs
230 were directly attached to activated or degenerate endothelium (Fig. 3F). Furthermore,
231 platelets were found between the pRBCs and endothelium (Fig. 3G). From these data,
232 we inferred that the depletion of phagocytes resulted in an increase in pRBCs attached
233 to the endothelia of capillaries, disrupting the microvascular blood flow and causing
234 pathological lesions in the liver and kidney.

235 **Increased parasite burden in the liver and kidney alters vascular endothelial**
236 **function.** The expression of adhesion molecules by vascular endothelial cells was
237 examined with qRT–PCR to assess their correlation with the parasite burden and
238 clinical complications. Strikingly, the expression of several endothelial biomarkers,
239 including ICAM1, vascular cell adhesion molecule 1 (VCAM1), platelet endothelial cell
240 adhesion molecule (PECAM), P-selectin, E-selectin, and Von Willebrand factor (vWF),
241 was significantly upregulated in the hepatic and renal tissues of the phagocyte-depleted
242 infected mice sampled on day 7 p.i. (Fig. 4A, B and Fig. S4). In contest, uninfected
243 mice treated with CLL showed no upregulation of the targeted genes (Fig. 4A, B and
244 Fig. S4), indicating that treatment with CLL didn't activate the endothelial cells. The
245 expression of ICAM1 and vWF, known to be predictors of severe malarial infection,
246 were then examined with immunohistochemistry. Consistent with the qRT-PCR results,
247 the staining patterns for ICAM1 and vWF in the vessels were markedly more intense in
248 livers and kidneys of the phagocyte-depleted infected mice than in those of the
249 PL-treated mice, which showed fewer and less intensely stained vessels (Fig. 4C, D).
250 Because vWF-expressing platelets mediate the adhesion of pRBCs to the endothelium
251 and the adhesion and aggregation of platelets at sites of vascular injury, leading to
252 thrombosis, we immunofluorescently stained the platelets with both anti-CD41 antibody

253 and anti-vWF antibody. Importantly, the renal sections from the phagocyte-depleted
254 infected mice, but not those from the PL-treated mice, displayed stronger expression of
255 both molecules at overlapping locations, indicating the accumulation of activated
256 platelets in the capillaries (Fig. 4E). Consistent with this, the phagocyte-depleted
257 infected mice showed significantly upregulated expression of platelet factor 4 (PF4), a
258 marker of platelet activation, in the renal tissues (Fig. 4F). Thus, the activation of the
259 endothelium was coincident with an increase in the adhesion/accumulation of both
260 pRBCs and the population of activated platelets in the renal vessels.

261 **Coagulation and inflammatory responses are elevated in phagocyte-depleted**
262 **infected mice.** Given the importance of activated platelets in initiating the coagulation
263 cascade and inflammatory response, several biomarker molecules were examined in the
264 tissues and blood of the mice. Importantly, the expression of the genes encoding TF (the
265 initiator of the extrinsic coagulation cascade), fibronectin (Fn), and vascular endothelial
266 growth factor (VEGF), markers of fibrosis, was upregulated in the renal tissues of the
267 phagocyte-depleted mice compared with that in the PL-treated mice on day 7 p.i. with *P.*
268 *yoelii* (Fig. 5A). Consistently, blood levels of coagulation factors, including Ptn, Fbg,
269 and DD, were significantly increased in the phagocyte-depleted mice on day 7 p.i. (Fig.
270 5B). We next examined the blood levels of IL-1β, IFN-γ, TNF-α, and IL-10, which are

271 known to play essential roles in the pathogenesis of malaria infection, as well as their
272 expressions in spleen tissues. Notably, the phagocyte-depleted mice exhibited
273 significantly increased levels of serum IL-1β, IFN-γ, and TNF-α (Fig. 5C), but not
274 IL-10 (data not shown) on day 7 p.i., compared with those in PL-treated mice. Similarly,
275 the expression of the genes encoding IFN-γ and TNF-α, but not IL-10, was upregulated
276 in the spleens of the phagocyte-depleted mice on day 7 p.i. (Fig. S5). The gene
277 expression of TGF-β was not detected in all samples of spleens (data not shown).
278 Collectively, these results demonstrated a correlation between glomerular fibrin
279 deposition, the activation of the coagulation and inflammatory responses in
280 phagocyte-depleted infected mice. Together, the depletion of phagocytes by using CLL
281 had resulted in an alternation of cellular population of spleen in *P. yoelii*-infected mice.
282 **Aspirin therapy attenuates the severity of *P. yoelii* infection in** phagocyte**-depleted**
283 **mice.** To clarify the mechanism of pathogenesis observed in our study, aspirin, an
284 antiplatelet drug, was used to reduce the serious vascular events attributable to severe
285 infection. Interestingly, the treatment of phagocyte-depleted mice with aspirin caused a
286 slight increase in their peripheral blood parasitemia, coincident with their improved
287 survival (Fig. 6A, B). In parallel, the parasite burden in the kidney, but not that in the
288 liver, was significantly reduced in the phagocyte-depleted mice treated with aspirin

289 compared with the phagocyte-depleted mice treated with PBS (Fig. 6C, D). Renal
290 lesions, including tubular necrosis and thrombi in the glomeruli, were also observed in
291 the infected phagocyte-depleted mice treated with either aspirin or PBS (Fig. S6).
292 However, the frequency of these lesions in the renal tissues was lower in the
293 aspirin-treated mice (30%, 3/10) than in the PBS-treated mice (60%, 6/10) after
294 infection with *P. yoelii*. Hepatic necrosis was also observed in the infected
295 phagocyte-depleted mice that were injected with aspirin (20%) or PBS (30%).
296 Consistent with the pathological observations, the serum levels of biochemical markers
297 of liver and kidney dysfunction were significantly elevated in the macrophage-depleted
298 mice compared with those in the PL-treated mice on day 7 p.i. However, the levels of
299 ALP, γGTP, AST, and BUN but not CRE were significantly lower in
300 phagocyte-depleted mice treated with aspirin than those treated with PBS (Fig. 6E).
301 Next, we examined the coagulation and inflammatory responses, the activation and
302 integrity of the endothelial cells, and the platelet activation in the renal tissues of the
303 infected mice after treatment with aspirin. The phagocyte-depleted infected mice
304 displayed significantly higher blood levels of Ptn, Fbg, DD, IFN-γ, TNF-α, and IL-1β
305 (Fig. 7) and greater expression of the genes for the activation of endothelial cells and
306 platelets than did the PL-treated mice on day 7 p.i. (Fig. S7). Importantly, the elevation

307 of these markers tended to be reduced in the infected phagocyte-depleted mice after
308 aspirin treatment while there was no statistically significant difference (Fig. 7 and Fig.
309 S7). These results showed that improved survival correlated strongly with a reduction in
310 the parasite burden in the renal tissues and was partially associated with the
311 coagulation/inflammatory responses and the activation of endothelial cells and platelets.
312

313 **DISCUSSION**

314 We have investigated the contribution of phagocytic cells including
315 macrophages to the protection against nonlethal infection of *P. yoelii* in mice. The
316 depletion of phagocytes in the acute-phase of *P. yoelii* infection, but not in the early- or
317 resolved-phase, impaired the resistance of C57BL/6 mice to the infection. The elevated
318 parasite burden in the liver and kidney of phagocyte-depleted mice was accompanied by
319 several pathophysiological features, including microvascular obstruction, increased
320 coagulation factors, and proinflammatory cytokines, and the activation of the
321 endothelium. An earlier study has shown that depletion of macrophages using two
322 injections of CLL in the early-phase of infection (days -2 and 3 post-infection) resulted
323 in an increased parasitemia of *P. yoelii* 17XNL-infected mice and rapid mortality as a
324 day earlier than control mice infected with lethal *P. yoelii* 17XL [13]. The differences in
325 these findings are most likely due to time of drug administration, number of injections
326 and dose of challenge infection. Likewise, Stevenson and colleagues has noted that
327 depletion of macrophages on day 6 post-infection with *P. chabaudi* AS was more
328 effective than depletion of macrophage in the early-phase of infection (day -1
329 post-infection) [14]. Here, single administration of CLL to *P. yoelii*-infected mice at
330 days 6 or 14 but not at days -2 or 30 post-infection showed severe pathogenesis in mice

331 typified by hepatic and renal failure. The severe pathogenesis after depletion of
332 phagocytes at the acute-phase of infection is most probably due to the high parasitemia
333 and abundant pRBCs with mature stage parasites that may sequestrate in the
334 microvascular and cause sudden disruption in the blood flow of organs [4].

335 Treatment with single injection of CLL in acute-phase of *P. yoelii* infection
336 resulted in a reduction in splenic population of macrophage, DC, granulocytes, NK and
337 $CD8^+$ T cells, and an increase in $CD4^+$ T cells. Likewise, naïve mice treated with CLL
338 had reduced the splenic population of macrophage, DC and $CD8^+$ T cells. This
339 treatment is known to mainly affect macrophage and DC in the marginal zone of spleen
340 as well as Kupffer cells in the liver [10]. Indeed, clodronate is specifically delivered into
341 phagocytic cells using liposomes as vehicles. Within these cells, phospholipid bilayers
342 of liposome are disrupted by lysosomal phospholipases and clodronate can be
343 intracellularly released and causes irreversibly damaged and death of cells by initiating
344 apoptosis [10]. Therefore, we believe that the impairment of the pRBCs clearance and
345 their particles in spleen by resident splenic phagocytic cells including macrophages
346 abrogated the resistance to non-lethal malarial infection. Nonetheless, the decrease in
347 splenic granulocytes and NK cells in infected mice is probably due to the loss of
348 macrophage and DCs that act as antigen presenting cells regulating the immune

349 response to the infection. The increase of $CD4^+$ T cells population might be caused by
350 the elevation of parasites burden and their antigens after depletion of phagocytic cells.
351 The $CD4^+$ T cells are known to be a key player in the protective immunity and the
352 pathogenesis of blood stage malaria infection. Moreover, $CD4^+CD25^+Foxp3^+$ regulatory
353 T cells are activated and expanded in response to malarial infection in mice and humans
354 to control proinflammatory immune responses upon *Plasmodium* infection [15, 16].
355 However, the contradictory findings in murine malaria suggested diverse roles of
356 regulatory T cells (protective or pathological) during infection [15, 16]. Therefore,
357 further study is needed to address the correlation between the regulatory T cells and the
358 severe pathogenesis in phagocyte-depleted mice.

359 Furthermore, phagocyte-depleted mice exhibited higher levels of IFN-γ, TNF-α,
360 and IL-1β, which are known to play important role in the protection and the
361 pathogenesis of malaria [17]. Therefore, the depletion of phagocytes not only impairs
362 the clearance of pRBCs but also alters the consequent immune responses to the
363 infection. Enhanced sequestration of parasitized RBC may then trigger inflammation
364 and cause concomitant enhancement of pro-inflammatory cytokine levels. Elevated
365 plasma IFN-γ, TNF-α and IL-1β cytokines in severe malaria are associated with
366 systemic complications and pathologic abnormalities in several organs. A clinical study

367 noted that renal failure in severe malaria is positively correlated with elevated blood
368 concentrations of TNF-α [18]. In support of this concept, TNF-α/β- or IFN-γ-deficient
369 mice are completely resistant to experimental cerebral malaria [19, 20]. Therefore,
370 further study is required to investigate the contribution of cytokines elevation to the
371 increased pathogenesis of malaria.

372 Phagocyte-depleted mice suffered acute renal failure, characterized by tubular
373 necrosis, glomerular thrombosis, mild fibrin deposition, and proteinuria, with elevated
374 levels of creatinine in the blood. The pathological lesions observed in moribund mice
375 may be due to the increased attachment of pRBCs in the glomerular capillaries that
376 triggers regional intravascular coagulation, blood hyperviscosity, and blood stasis.
377 These results are consistent with concept that the outcome of severe malarial infection
378 depends on the degree of sequestration and accumulation of pRBCs in the
379 microvasculature of vital organs [21, 22]. The absence of electron-dense deposits in the
380 basement membranes of the glomerular capillaries and monocyte infiltration into the
381 glomerular capillaries indicates that the underlying mechanism of acute renal failure in
382 our mouse model is not immune-complex-mediated glomerulonephritis. In an analogous
383 fashion, acute renal failure has frequently been reported to be a serious complication of
384 *P. falciparum* and *P. vivax* malaria in nonimmune adults and children in Africa and

385 Southeast Asia [23, 24]. Renal ischemia arising from the sequestration of pRBCs in the
386 glomerular and tubulointerstitial capillaries is believed to be the major key
387 pathophysiology related to acute renal failure in humans and experimental animals [25,
388 26]. Moreover, patients suffering from acute renal failure arising from malarial infection
389 may display oliguria, proteinuria, hyperbilirubinemia, and high levels of plasma
390 creatinine [27, 28]. Renal biopsies of patients show acute tubular necrosis,
391 tubulointerstitial nephritis, and glomerular changes with mesangial proliferation, with or
392 without immune complex deposition. Glomerular hypercellularity, typified by the
393 sequestration of pRBCs with or without the accumulation of monocytes in the
394 glomerular capillaries, is a common pathological feature in these patients [29, 30].
395 Fibrin deposition in the glomeruli has also been observed postmortem in some malarial
396 patients [29]. Together, the high degree of pathophysiological similarity between our
397 findings and those for human malaria patients suffering from renal failure highlights the
398 importance of our model for investigating novel strategies for therapeutic interventions.

399 Fibrin and thrombi in the glomerular capillaries are the most common
400 pathological feature of many renal diseases characterized by the interruption of blood
401 flow, irreversible ischemia, and necrosis. The mechanism of fibrin deposition in the
402 small arteries and glomerular capillaries has been shown to depend on the interaction

403 between endothelial cells and the macrophages or platelets that initiate thrombosis and
404 fibrosis [29, 30]. However, phagocyte-depleted mice exhibited an increase in the
405 number of activated platelets, which is most probably due to the elevation in parasites
406 burden and cytokines production as well as the endothelial damage in liver and kidney.
407 Generally, the direct interaction/communication between activated platelets and the
408 inflamed endothelium mounts a coagulation response via the amplification of thrombin
409 from TF, leading to fibrin deposition in the glomerular capillaries and arterioles [6, 30].
410 In our study, therefore, the aggregation of pRBCs, dpRBCs, and activated platelets in
411 the inflamed microvasculature of the renal tissues coincided with increased coagulation
412 and inflammatory responses in the CLL-treated mice may explain the observation of
413 thrombi and fibrin deposition in the capillaries. Consistent with this notion, platelet
414 adhesion and aggregation are known to play important roles in cerebral malaria by
415 facilitating the cytoadhesion of *P. falciparum* pRBCs to the activated endothelium [31].
416 Platelets respond rapidly to pRBCs, forming aggregations of pRBCs and platelets via
417 vWF, which then attach firmly to the inflamed endothelia by their surface adhesion
418 molecules [32, 33]. The upregulated expression of adhesive ligands of platelets
419 stabilizes plug formation and recruits other cells, resulting in microvascular obstruction
420 with or without fibrin deposition [6, 31]. Concurrently, malarial patients display

421 thrombocytopenia, resulting from the sequestration/aggregation of activated platelets to
422 the vascular endothelium and the removal of platelet-bound pRBCs from the blood by
423 phagocytosis [5]. Together, these findings suggest that the inadequate removal of
424 aggregated platelets and pRBCs by phagocytes results in microvascular obstruction in
425 the vital organs, such as the kidney, thus causing severe malaria.

426 Because platelets are crucial in initiating the coagulation cascade, we presumed
427 that the blockage of platelet activation by aspirin may reduce the
428 coagulation–inflammation responses. Our results demonstrated that treatment with
429 aspirin attenuated the severity of *P. yoelii* infection in phagocyte-depleted mice, which
430 was evidenced by their improved survival. The phagocyte-depleted mice treated with
431 aspirin displayed a reduced parasite burden in the kidney, with fewer renal lesions than
432 the phagocyte-depleted mice treated with PBS. A possible interpretation of the
433 improved survival of the phagocyte-depleted mice after treatment with aspirin is that
434 fewer pRBCs were sequestered to the glomerular capillaries because platelet
435 aggregation, the binding of pRBCs and platelets to the endothelium were disrupted by
436 aspirin. However, these results emphasize that phagocytic cells including macrophages
437 are the central determinants of the infection outcome, probably by mediating the
438 clearance of pRBCs and aggregated platelets.

439 In conclusion, our data imply that severe malarial infection in patients and
440 experimental animals may be attributable to the inappropriate function of phagocytic
441 cells including macrophages in the removal of pRBCs, leading to their excessive
442 sequestration and impairment of the microvascular blood flow.
443

Acknowledgments

We thank Dr. Motomi Torii (Department of Molecular Parasitology, Ehime University School of Medicine, Japan) for providing *P. yoelii* 17XNL. We thank Youko Matsushita, Megumi Noda, and Yoshie Imura (National Research Center for Protozoan Diseases, Obihiro University of Agriculture and Veterinary Medicine) for their excellent technical assistance. We sincerely thank Dr. Satoru Kawai (Center for Tropical Medicine and Parasitology, Dokkyo Medical University) for his helpful advice and discussion of the electron microscopy study. This research was supported by the Japan Society for the Promotion of Science (JSPS) through the Funding Program for Next-Generation World-Leading Researchers (NEXT Program), initiated by the Council for Science and Technology Policy (2011/LS003).

456 **REFERENCES**

457 1. **Miller LH, Baruch DI, Marsh K, Doumbo OK.** 2002. The pathogenic basis of
458 malaria. Nature **415**: 673-679.
459 2. **Miller LH, Ackerman HC, Su XZ, Wellems TE.** 2013. Malaria biology and
460 disease pathogenesis: insights for new treatments. Nat Med **19:**156-167.
461 3. **Schofield L, Grau GE.** 2005. Immunological processes in malaria pathogenesis.
462 Nat Rev Immunol **5**:722-735.
463 4. **Dondorp AM, Ince C, Charunwatthana P, Hanson J, van Kuijen A, Faiz MA,**
464 **Rahman MR, Hasan M, Bin Yunus E, Ghose A, Ruangveerayut R,**
465 **Limmathurotsakul D, Mathura K, White NJ, Day NP.** 2008. Direct in vivo
466 assessment of microcirculatory dysfunction in severe falciparum malaria. J Infect
467 Dis **197**:79-84.
468 5. **Faille D, El-Assaad F, Alessi MC, Fusai T, Combes V, Grau GE.** 2009.
469 Platelet-endothelial cell interactions in cerebral malaria: the end of a cordial
470 understanding. Thromb Haemost **102**:1093-1102.
471 6. **Francischetti IM, Seydel KB, Monteiro RQ.** 2008. Blood coagulation,
472 inflammation, and malaria. Microcirculation **15**:81-107.

473 7. **Vogetseder A, Ospelt C, Reindl M, Schober M, Schmutzhard E.** 2004. Time
474 course of coagulation parameters, cytokines and adhesion molecules in *Plasmodium*
475 *falciparum* malaria. Trop Med Int Health **9**:767-773.
476 8. **Engwerda CR1, Beattie L, Amante FH.** 2005. The importance of the spleen in
477 malaria. Trends Parasitol **21**:75-80.
478 9. **Buffet PA, Safeukui I, Deplaine G, Brousse V, Prendki V, Thellier M, Turner**
479 **GD, Mercereau-Puijalon O.** 2011. The pathogenesis of *Plasmodium falciparum*
480 malaria in humans: insights from splenic physiology. Blood **117**:381-392.
481 10. **Aichele P, Zinke J, Grode L, Schwendener RA, Kaufmann SH, Seiler P.** 2003.
482 Macrophages of the splenic marginal zone are essential for trapping of blood-borne
483 particulate antigen but dispensable for induction of specific T cell responses. J
484 Immunol **171**:1148-1155.
485 11. **van Rooijen N, Hendrikx E.** 2010. Liposomes for specific depletion of
486 macrophages from organs and tissues. Methods Mol Biol **605**:189-203.
487 12. **McMorran BJ, Marshall VM, de Graaf C, Drysdale KE, Shabbar M, Smyth**
488 **GK, Corbin JE, Alexander WS, Foote SJ.** 2009. Platelets kill intraerythrocytic
489 malarial parasites and mediate survival to infection. Science **323**:797-800.

490 13. **Couper KN, Blount DG, Hafalla JC, van Rooijen N, de Souza JB, Riley EM.**
491 2007. Macrophage-mediated but gamma interferon-independent innate immune
492 responses control the primary wave of *Plasmodium yoelii* parasitemia. Infect
493 Immun **75**:5806–5818.
494 14. **Stevenson MM, Ghadirian E, Phillips NC, Rae D, Podoba JE.** 1989. Role of
495 mononuclear phagocytes in elimination of *Plasmodium chabaudi* AS infection.
496 Parasite Immunol **11**:529-544.
497 15. **Scholzen A, Minigo G, Plebanski M.** 2010. Heroes or villains? T regulatory cells
498 in malaria infection. Trends Parasitol **26**:16-25.
499 16. **Hansen DS, Schofield L.** 2010. Natural regulatory T cells in malaria: host or
500 parasite allies? PLoS Pathog. **29**:e1000771.
501 17. **Angulo I, Fresno M.** 2002. Cytokines in the pathogenesis of and protection against
502 malaria. Clin Diagn Lab Immunol **9**:1145-1152.
503 18. **Day NP, Hien TT, Schollaardt T, Loc PP, Chuong LV, Chau TT, Mai NT, Phu**
504 **NH, Sinh DX, White NJ, Ho M.** 1999. The prognostic and pathophysiologic role
505 of pro- and antiinflammatory cytokines in severe malaria. J Infect Dis
506 **180**:1288-1297.

507 19. **Rudin W, Eugster HP, Bordmann G, Bonato J, Müller M, Yamage M, Ryffel**
508 **B.** 1997. Resistance to cerebral malaria in tumor necrosis
509 factor-alpha/beta-deficient mice is associated with a reduction of intercellular
510 adhesion molecule-1 up-regulation and T helper type 1 response. Am J Pathol.
511 **150**:257-266.
512 20. **Rudin W, Favre N, Bordmann G, Ryffel B.** 1997. Interferon-gamma is essential
513 for the development of cerebral malaria. Eur J Immunol **27**:810-815.
514 21. **Baptista FG, Pamplona A, Pena AC, Mota MM, Pied S, Vigário AM.** 2010.
515 Accumulation of *Plasmodium berghei*-infected red blood cells in the brain is
516 crucial for the development of cerebral malaria in mice. Infect Immun
517 **78**:4033-4039.
518 22. **Haque A, Best SE, Amante FH, Ammerdorffer A, de Labastida F, Pereira T,**
519 **Ramm GA, Engwerda CR.** 2011. High parasite burdens cause liver damage in
520 mice following *Plasmodium berghei* ANKA infection independently of CD8(+) T
521 cell-mediated immune pathology. Infect Immun **79**:1882-1888.
522 23. **Naqvi R, Ahmad E, Akhtar F, Naqvi A, Rizvi A.** 2003. Outcome in severe acute
523 renal failure associated with malaria. Nephrol. Dial. Transplant **18**:1820-1823.

524 24. **Elsheikha HM, Sheashaa HA.** 2007. Epidemiology, pathophysiology,
525 management and outcome of renal dysfunction associated with plasmodia infection.
526 Parasitol Res **101**:1183-1190.
527 25. **Houba V.** 1979. Immunologic aspects of renal lesions associated with malaria.
528 Kidney Int **16**:3–8.
529 26. **Ehrich JH, Eke FU.** 2007. Malaria-induced renal damage: facts and myths. Pediatr
530 Nephrol **22**:626-637.
531 27. **Sowunmi A.** 1996. Renal function in acute *falciparum* malaria. Arch Dis Child
532 **74**:293-298.
533 28. **Nguansangiam S, Day NP, Hien TT, Mai NT, Chaisri U, Riganti M, Dondorp**
534 **AM, Lee SJ, Phu NH, Turner GD, White NJ, Ferguson DJ, Pongponratn E.**
535 2007. A quantitative ultrastructural study of renal pathology in fatal *Plasmodium*
536 *falciparum* malaria. Trop Med Int Health **12**:1037-1050.
537 29. **Boonpucknavig V, Sitprija V.** 1979. Renal disease in acute *Plasmodium*
538 *falciparum* infection in man. Kidney Int **16**:44-52.
539 30. **Hertig A, Rondeau E.** 2004. Role of the coagulation/fibrinolysis system in
540 fibrin-associated glomerular injury. J Am Soc Nephrol **15**:844-853.

31. **Cox D, McConkey S.** 2010. The role of platelets in the pathogenesis of cerebral malaria. Cell Mol Life Sci **67**:557-568.

32. **Larkin D, de Laat B, Jenkins PV, Bunn J, Craig AG, Terraube V, Preston RJ, Donkor C, Grau GE, van Mourik JA, O'Donnell JS.** 2009. Severe *Plasmodium falciparum* malaria is associated with circulating ultra-large von Willebrand multimers and ADAMTS13 inhibition. PLoS Pathog **5**:e1000349. doi:10.1371/journal.ppat.1000349.

33. **Francischetti IM, Seydel KB, Monteiro RQ, Whitten RO, Erexson CR, Noronha AL, Ostera GR, Kamiza SB, Molyneux ME, Ward JM, Taylor TE.** 2007. *Plasmodium falciparum*-infected erythrocytes induce tissue factor expression in endothelial cells and support the assembly of multimolecular coagulation complexes. J Thromb Haemost **5**:155-165.

555 **Figure legends**

556 **Fig. 1. Parasitemia and survival of *P. yoelii*-infected mice.** Mice were injected with
557 clodronate liposomes (CLL) or PBS liposomes (PL) on day –2 p.i. (A, B), day 6 p.i. (C,
558 D), or day 14 p.i. (E, F) and then monitored for 30 days for parasitemia (A, C, E) and
559 survival (B, D, F). Infected mice with no treatment (NT). The results represent the
560 average parasitemia and survival of mice (n =10 for A, B, E, F; n = 15 for C, D; n = 5
561 for NT mice). Data are combined from two or three independent experiments. *
562 Indicates the significant difference in the parasitemia of CLL-treated mice as compared
563 with control mice as analyzed by two-way ANOVA. Arrowheads indicate the time for
564 administration of CLL or PL.

565 **Fig. 2. Hepatic and renal failure in *P. yoelii*-infected mice.** Biochemical analysis of
566 serum markers of liver and kidney function (A). Samples were collected on day 7 p.i.
567 from *P. yoelii*-infected mice treated with either PBS liposomes (PL) or clodronate
568 liposomes (CLL) on day 6 p.i. Uninfected mice were treated with PBS liposomes (CPL)
569 or clodronate liposomes (CCLL) and sampled one day after treatment. The results
570 represent the average value (± SEM) for each experimental group (uninfected, n = 5;
571 infected, n = 15). * Indicates the significant difference between the groups as analyzed
572 by one-way ANOVA analysis of variance, followed by Tukey's multiple-comparison

573 test. U/L, unit/L; ALP, alkaline phosphatase; γ-GTP, γ-glutamyl transpeptidase; AST,
574 aspartate transaminase; BUN, blood urea nitrogen; CRE, creatinine. Histopathological
575 observations of hepatic and renal tissues of *P. yoelii*-infected mice (B-E). Tissues were
576 sampled for histopathological studies on day 7 p.i. after treatment with clodronate
577 liposomes (CLL) or PBS liposomes (PL) on day 6 p.i. Hepatic sections (B) and renal
578 sections (C–E). Infected macrophage-depleted mice (CLL) showed focal hepatic
579 necrosis (B), tubular necrosis (C), blood stasis (D), and fibrin deposition in the
580 glomeruli (E). HE staining (B–D), PTAH staining (E). Arrowheads indicate lesions.
581 Scale bars are indicated.

582 **Fig. 3. Parasite burden in the livers and kidneys of *P. yoelii*-infected mice.** Tissues
583 were sampled on day 7 p.i. after mice were treated with either clodronate liposomes
584 (CLL) or PBS liposomes (PL) on day 6 p.i. Analysis of the relative expression of *P.*
585 *yoelii* 18S rRNA by qRT–PCR in hepatic (A) and renal (B) tissues. Results represent
586 the $2^{-\Delta\Delta Ct}$ average of relative expression (± SEM) of the parasite gene in mice (n = 15)
587 relative to that in PL-treated mice. Data are combined from three independent
588 experiments. * Indicates the significant difference between the groups as analyzed by
589 Student's *t* test. Specific immunofluorescent staining of the parasite using antiserum
590 directed against PyMSP-1 in the liver (C) and kidney (D). Ultrastructural examination

591 of renal sections from phagocyte-depleted infected mice (E–G). Electron micrograph of
592 a glomerular capillary lumen filled with RBCs, parasitized RBCs (pRBCs), and
593 degenerate pRBCs (dpRBCs) (E), apparently attached to the degenerate endothelium (F).
594 Platelets were found between pRBCs and the endothelium (G). EC, endothelial cells;
595 BM, basement membrane; PLT, platelets. Scale bars are indicated.

596 **Fig. 4. mRNA expression and immunohistochemical analyses of endothelial**
597 **markers in hepatic and renal tissues**. Gene expression of endothelial-cell adhesion
598 molecules in hepatic (A) and renal tissues (B). Samples from *P. yoelii*-infected mice
599 treated with either PBS liposomes (PL) or clodronate liposomes (CLL) on day 6 p.i.
600 were collected on day 7 p.i. Uninfected mice were treated with PBS liposomes (CPL) or
601 clodronate liposomes (CCLL) and sampled one day after treatment. The results
602 represent the $2^{-\Delta\Delta Ct}$ average of relative expression (± SEM) of each targeted gene in the
603 mice (uninfected, n = 5; infected, n = 15) relative to that of the corresponding gene in
604 uninfected mice treated with PBS liposomes (CPL). * Indicates the significant
605 difference between the groups as analyzed by one-way ANOVA analysis of variance.
606 Immunohistochemical observations (C-E). Sections of liver (C) and kidney (D) were
607 stained with specific antibody directed against ICAM1 or vWF. Specific
608 immunofluorescent staining for activated endothelial cells/platelets and platelets in renal

609 tissues using antibodies directed against vWF and CD41 (E). Scale bars are indicated.
610 Expression of PF4, an platelet activation marker in renal tissues (F). The results
611 represent the $2^{-\Delta\Delta Ct}$ average of relative expression (± SEM) of each targeted gene in the
612 mice (uninfected, n = 5; infected, n = 15) relative to that of the corresponding gene in
613 uninfected mice treated with PBS liposomes (CPL). * Indicates the significant
614 difference between the groups as analyzed by one-way ANOVA analysis of variance,
615 followed by Tukey's multiple-comparison test.

616 **Fig. 5. Expression and serum levels of coagulation factors and serum inflammatory**
617 **cytokine in *P. yoeli*-infected mice.** Expression of coagulation and damage markers in
618 renal tissues (A). The results represent the $2^{-\Delta\Delta Ct}$ average of relative expression (± SEM)
619 of each targeted gene in the mice (uninfected, n = 5; infected, n = 15) relative to that of
620 the corresponding gene in uninfected mice treated with PBS liposomes (CPL).
621 Serological detection of coagulation factors (B) and inflammatory cytokines (C). *P.*
622 *yoelii*-infected mice treated with either PBS liposomes (PL) or clodronate liposomes
623 (CLL) on day 6 p.i. were collected on day 7 p.i. Uninfected mice were treated with PBS
624 liposomes (CPL) or clodronate liposomes (CCLL) and sampled one day after treatment.
625 * Indicates the significant difference between the groups as analyzed by one-way
626 ANOVA analysis of variance, followed by Tukey's multiple-comparison test.

627 **Fig. 6. Effects of aspirin treatment on the outcomes of infection with *P. yoelii*.**
628 Parasitemia (A) and survival (B) of mice in the 30 days after infection. The results
629 represent the average parasitemia ± SEM of the mice (n = 10). Parasite burden in
630 hepatic (C) and renal (D) tissues as examined qRT–PCR. Relative gene expression of *P.*
631 *yoelii* 18S rRNA in the livers (C) and kidneys (D) of infected mice sampled on day 7 p.i.
632 The results represent the $2^{-\Delta\Delta Ct}$ average of relative expression (± SEM) of the infected
633 mice (n = 10) relative to that in PBS liposomes-treated and PBS-injected mice
634 (PL(PBS)). Biochemical analysis of serum markers of liver and kidney function in
635 infected mice (E). Mice were either injected with clodronate liposomes (CLL) or PBS
636 liposomes (PL) on day 6 p.i. and were also treated with either aspirin or PBS from day 5
637 to day 8 p.i. * Indicates the significant difference between the groups as analyzed by
638 one-way ANOVA analysis of variance, followed by Tukey's multiple-comparison test.
639 **Fig. 7. Effects of aspirin treatment on serum levels of coagulation factors and**
640 **inflammatory cytokines.** Mice were either injected with clodronate liposomes (CLL)
641 or PBS liposomes (PL) on day 6 p.i. and were also treated with either aspirin (gray
642 column) or PBS (black column) on days 5 and 6 p.i., and sampled for analyses on day 7
643 p.i. The results represent the average values (± SEM) of the mice (n = 10). * Indicates
644 the significant difference between the groups as analyzed by one-way ANOVA analysis

645 of variance, followed by Tukey's multiple-comparison test.

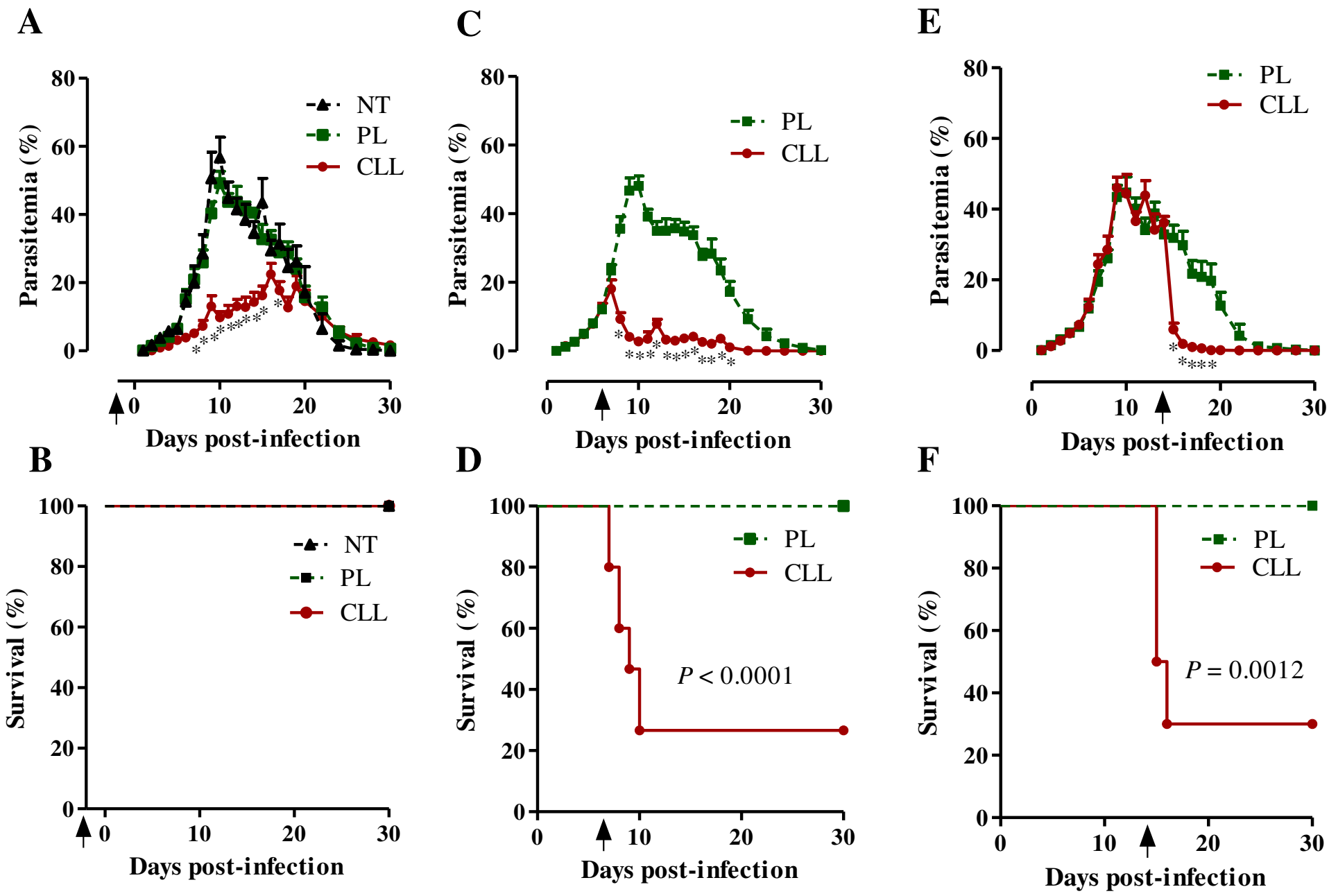
A
B
C
D
E
F
Parasitemia (%)
Survival (%)
Days post-infection
NT
PL
CLL
P < 0.0001
P = 0.0012

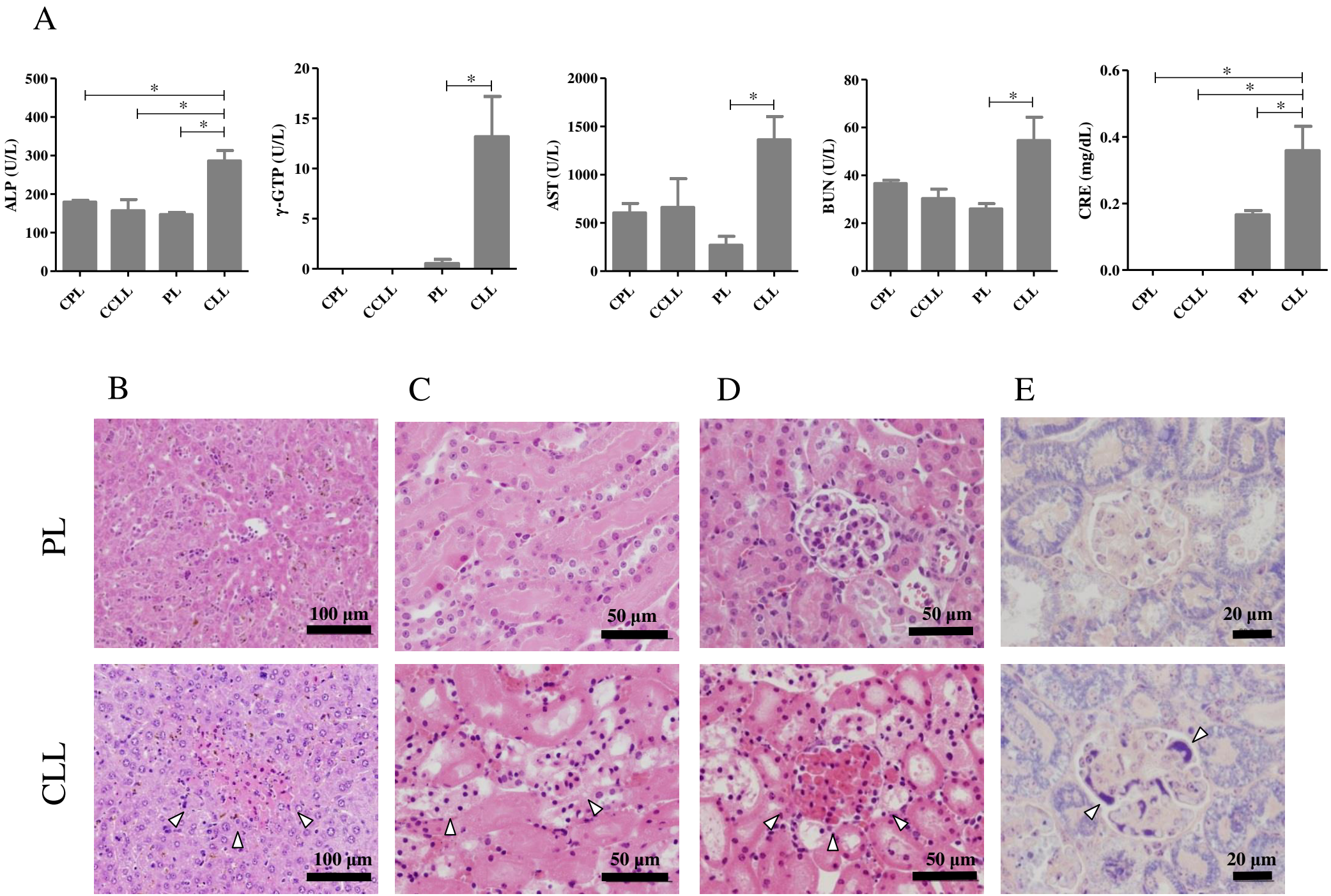
A
ALP (U/L)
γ-GTP (U/L)
AST (U/L)
BUN (U/L)
CRE (mg/dL)
CPL
CCLL
PL
CLL
B
C
D
E
PL
CLL
100 μm
50 μm
20 μm

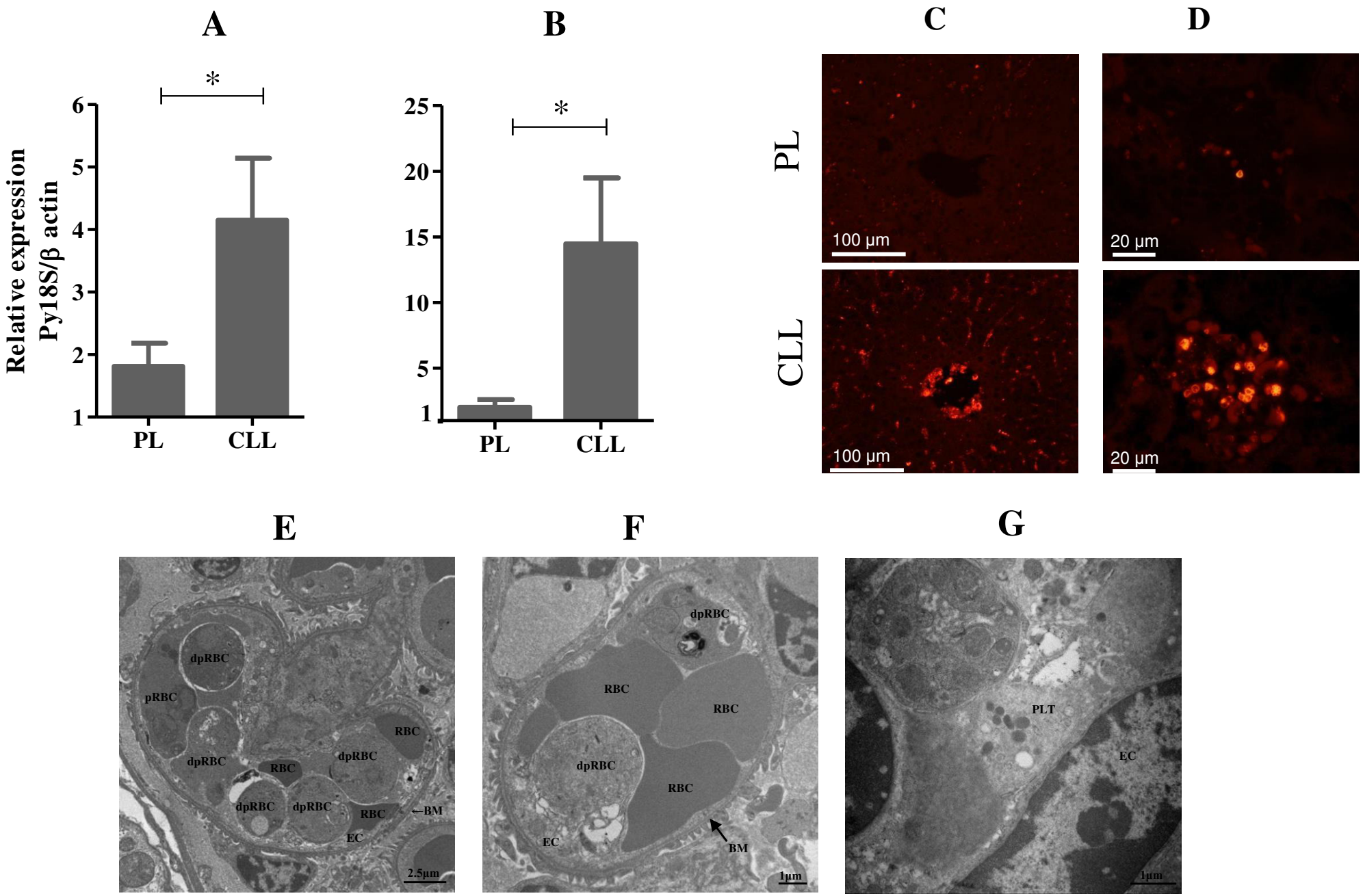
A
B
C
D
E
F
G
Relative expression
Py18S/β actin
*
PL
CLL
100 µm
20 µm
dpRBC
pRBC
RBC
EC
←BM
2.5µm
BM
1µm
PLT

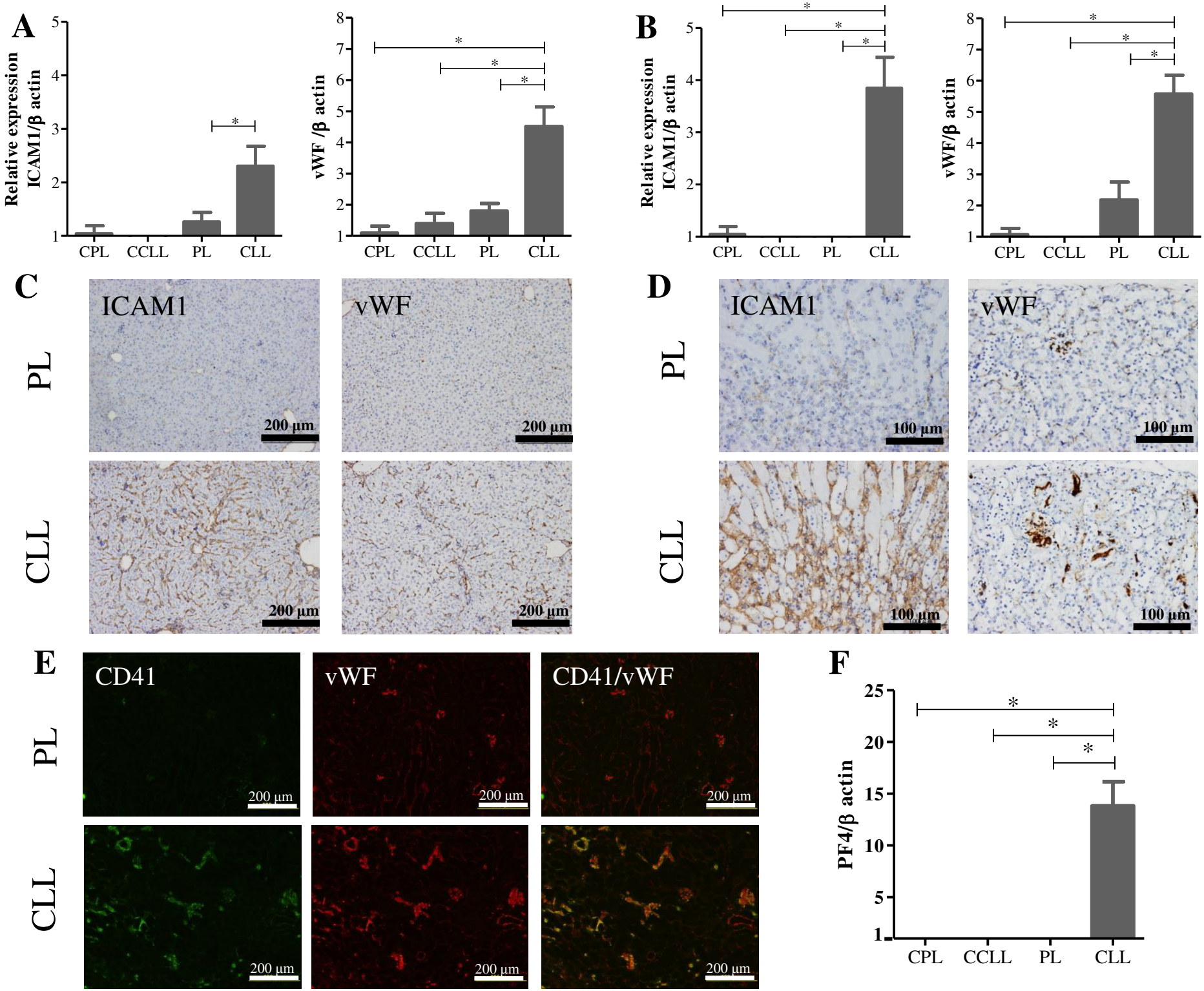
A
Relative expression ICAM1/β actin
vWF /β actin
CPL
CCLL
PL
CLL
B
Relative expression ICAM1/β actin
vWF/β actin
C
ICAM1
vWF
PL
CLL
200 μm
D
100 μm
E
CD41
vWF
CD41/vWF
F
PF4/β actin

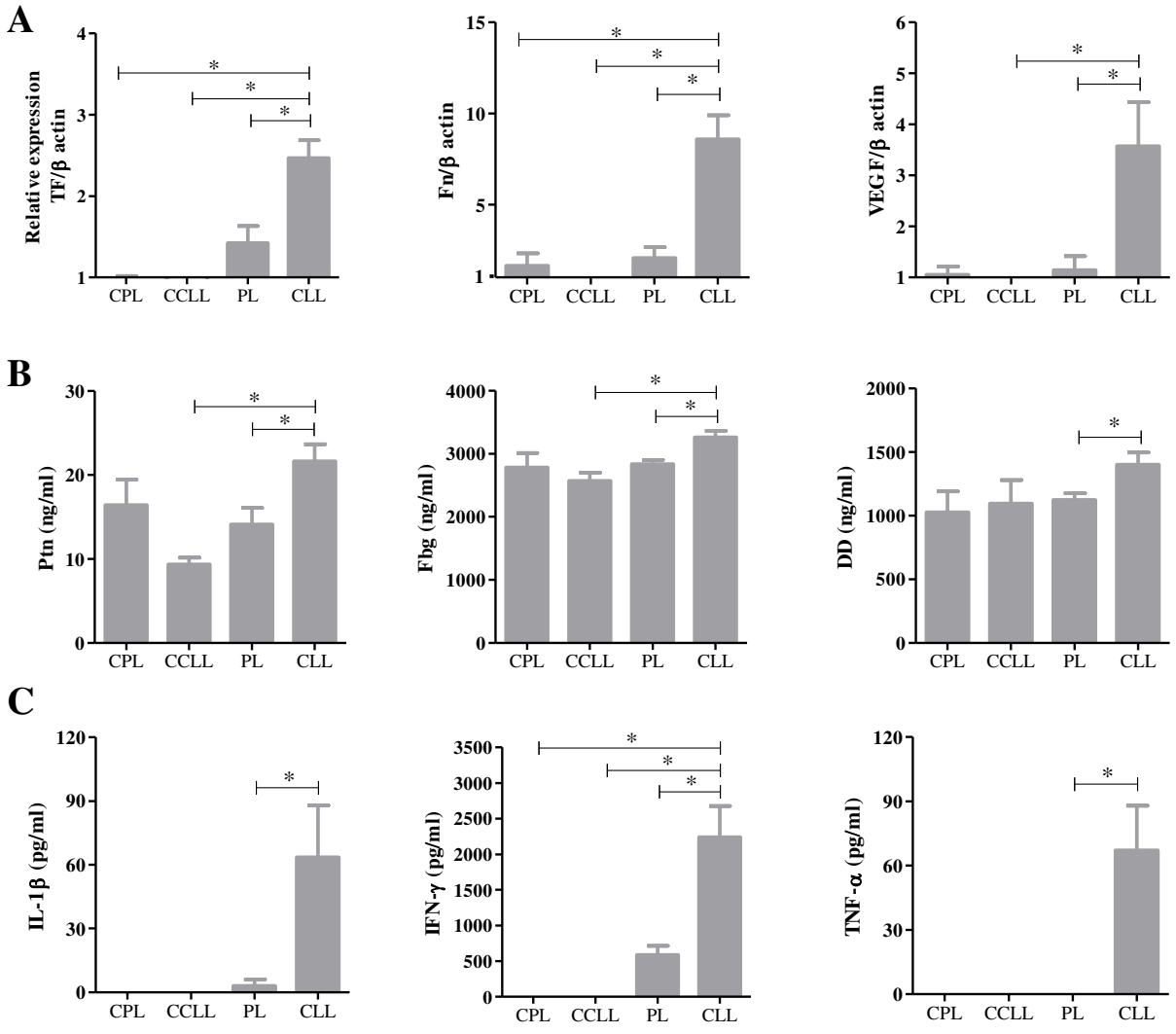
A
Relative expression TF/β actin
Fn/β actin
VEGF/β actin
B
Ptn (ng/ml)
Fbg (ng/ml)
DD (ng/ml)
C
IL-1β (pg/ml)
IFN-γ (pg/ml)
TNF-α (pg/ml)
CPL
CCLL
PL
CLL
*

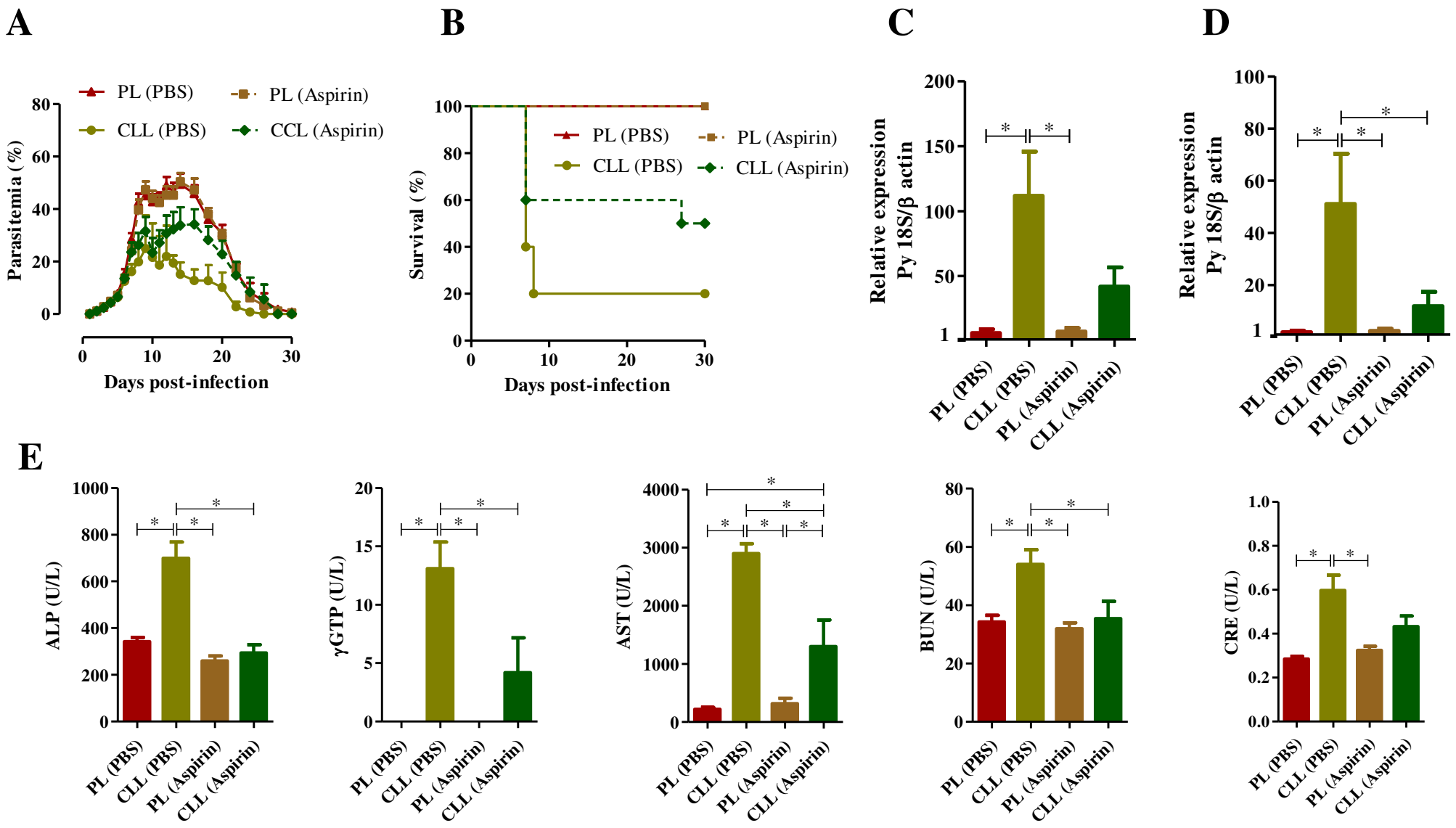
A
PL (PBS)
PL (Aspirin)
CLL (PBS)
CCL (Aspirin)
Parasitemia (%)
Days post-infection
B
PL (PBS)
PL (Aspirin)
CLL (PBS)
CLL (Aspirin)
Survival (%)
Days post-infection
C
Relative expression
Py 18S/β actin
PL (PBS)
CLL (PBS)
PL (Aspirin)
CLL (Aspirin)
D
Relative expression
Py 18S/β actin
PL (PBS)
CLL (PBS)
PL (Aspirin)
CLL (Aspirin)
E
ALP (U/L)
γGTP (U/L)
AST (U/L)
BUN (U/L)
CRE (U/L)
PL (PBS)
CLL (PBS)
PL (Aspirin)
CLL (Aspirin)

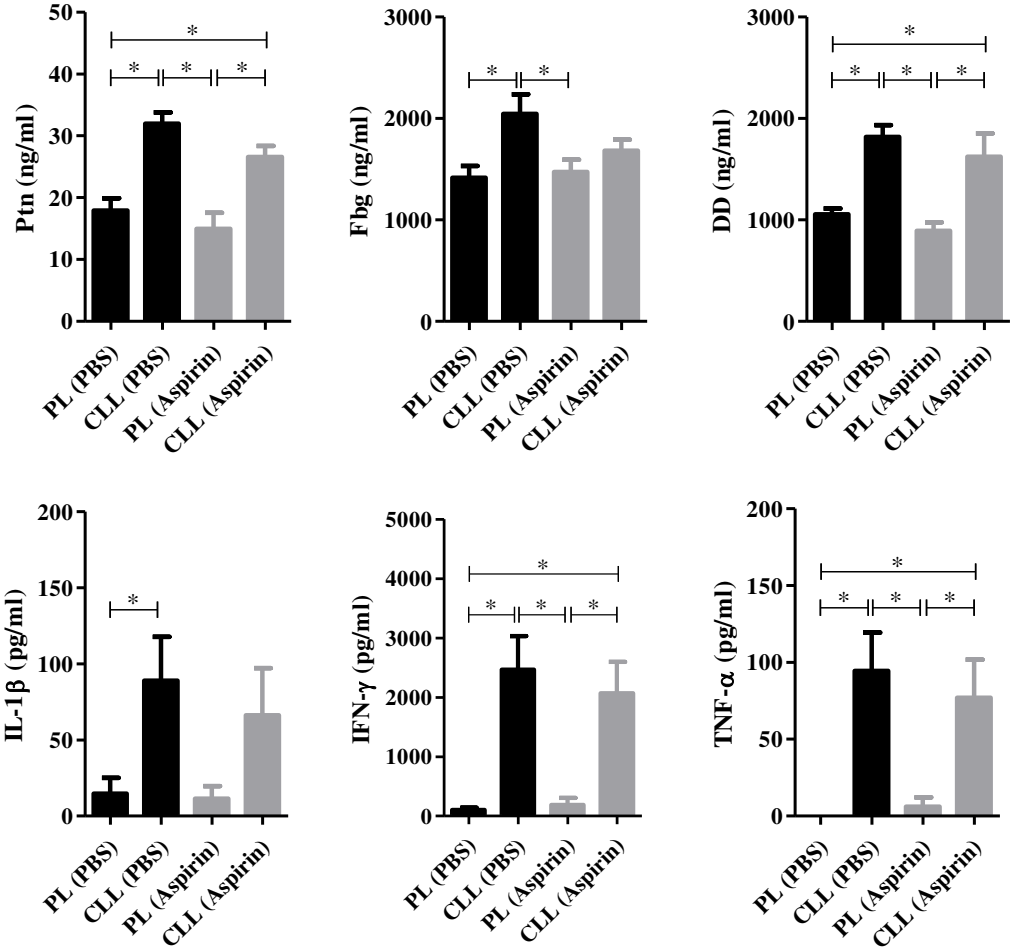
Ptn (ng/ml)
Fbg (ng/ml)
DD (ng/ml)
IL-1β (pg/ml)
IFN-γ (pg/ml)
TNF-α (pg/ml)
PL (PBS)
CLL (PBS)
PL (Aspirin)
CLL (Aspirin)
*